

High-Frequency Bistatic Scattering from a Corrugated Sediment Surface

Hongsang Cho*, Hyoungsul La*, Kwan-seob Yoon*, Jungyul Na*, Bong-chae Kim**

*Department of Earth & Marine Sciences, Hanyang University

**Korea Ocean Research and Development Institute

(Received April 25 2006; Revised Jun 7 2006; Accepted Jun 10 2006)

Abstract

High-frequency bistatic scattering measurements from a corrugated surface were made in an acoustic water tank. First the azimuthal scattering pattern was measured from an artificially corrugated surface which has varying impedance. The corrugated surface was installed both transverse to the direction of incident wave and longitudinal to the direction of incident wave. The angle between the corrugated surface and the direction of the incident wave was about 45°. Second, the scattering strengths were measured from the flat sediment and the corrugated sediment. A critical angle of about 37° was calculated in the acoustic water tank. The measurements were made at three fixed grazing angles: 33° (lower than critical angle), 37° (critical angle), and 41° (higher than critical angle). The scattering angle and the grazing angle are equal in each measurement. Frequencies were from 50 kHz to 100 kHz with an increment of 1 kHz. The corrugated sediment was made transverse to the direction of the incident wave. The first measurement indicates that the scattering patterns depend on the relations between the corrugated surface and the direction of the incident wave. In the second measurement, the data measured from the flat sediment were compared to the APL-UW model and to the NRL model. The NRL model's output shows more favorable comparisons than the APL-UW model. In case of the corrugated sediment, the model and the measured data are different because the models used an isotropic wave spectrum of sediment roughness in the scattering calculations. The isotropic wave spectrum consists of w_2 and γ_2 . These constants derived from sediment names or bulk size. The model which used the constants didn't consider the effect of a corrugated surface. In order to consider a corrugated surface, the constants were varied in the APL-UW model.

Keywords: Bistatic, Bottom scattering, scattering model, Corrugated surface, Bottom scattering model

I. Introduction

Ocean bottoms may be considered locally as a plane, on average, with a microscale roughness whose influence will be significant if its characteristic dimensions are at least comparable in magnitude to the acoustic wavelength [1]. The effect of the bottom relief on the incident acoustic wave will be a compound of the frequency, the angle of incidence and the local

characteristics of the relief. Microscale roughness has various possible origins. On the bottom, the roughness depends on the geology (strong relief on rock, tide and current ripples, and living organisms on or in the sand or mud). The microscale roughness presents a wide scale of amplitudes. For processes that are of interest at sonar frequencies, these amplitudes range between a millimeter and a few meters. When the water depth is shallow enough, wave-induced currents on the bottom will produce directional sand ripples. These ripples contain information about wave conditions and direction, water depth and environment. In this case, the two roughness scales might correspond to different

Corresponding author: Jungyul Na (najy0252@hanyang.ac.kr)

Department of Earth & Marine Sciences Hanyang University, Sang Rok Gu, Ansan, Kyunggi-do

physical processes, depending on their size relative to the acoustic wavelength.

When a sound beam is incident on a rough ocean and sand ripple bottom, it is scattered in all directions by surface roughness and sediment inhomogeneities. This angular spread of scattered signals can significantly degrade the performance of active high-frequency sonar systems. Because of their cost and complexity, only a few high-resolution bistatic scattering measurements have been made and no large angle high-frequency bistatic scattering measurements have been reported.

Typically, shallow-water bottom backscattering measurements have been made using monostatic configurations. These measurements have been made as a function of frequency, grazing angle, azimuthal angles and environmental conditions. Stanic, et al. [2] and Boehme, et al. [3] have made bottom backscattering measurements as a function of azimuthal angles, but these measurements were made using monostatic configurations. Nolle, et al. [4] has made bottom backscattering measurements in a sand-filled laboratory tank. Even though these measurements were made using a separate source and receiver, no discussions of bistatic scattering strengths were done. Urick [5] made the earliest series of shallow-water bistatic bottom scattering measurements. These measurements were made south of Panama City at a frequency of 22 kHz. Those results showed that bottom backscattering strengths varied randomly between -30 and -40 dB, with no noticeable dependence on bistatic scattering angle. Stanic, et al. [2] made bistatic bottom scattering measurements in an area 26 miles east of Jacksonville, Florida. These measurements were made using a receiving array. The results indicated that bistatic variability tends to decrease with a decreasing grazing angle and to show only weak frequency dependence. Recently, Choi, et al. [6] made measurements from naturally formed ripple bottoms off the coast of Ducksan port near Donghea City. The scattering characteristics showed an augmented out-of-plane scattering dependent on the ripple aspect.

This paper presents results from measurement of high-frequency bistatic scattering from corrugated sediment surface. The measured data were compared to the APL-UW and the NRL models. In these models, the surface roughness is defined in terms of its PDF of displacements above and below the mean, or in terms of the rms deviation from the mean height. The spatial frequency spectrum of the displacements and the directional wave spectrum are closely related to the scattering of sound from the rough surface. The spatial frequency spectrum can be written as $W(k) = w_2 K^{-\gamma_2}$, where $W(k)$ is the power spectral density, k is

the spatial cycle frequency and w_2 and γ_2 are constants. A variety of constants (w_2 , γ_2) may be used to describe these surface properties. Usually, the sediment name or bulk size had represented the surface properties, therefore the model isn't considered a corrugated surface. For that reason, a variety of model constants is used to increase the correlation between the model and the measured data.

II. Bistatic scattering model

The theory of acoustic scattering by the bottom has been the subject of numerous investigations over the last 40 years. During this period many theories have been developed. The two approximations most commonly used in the theory of wave scattering from rough surfaces are perturbation [8] and the Kirchhoff approximation [9]. Perturbation approximation is valid for small radii curvature, provided that the interface relief is much smaller than the acoustic wavelength. The first of these restrictions arises from the assumption that quantities that are functions of surface height may be expanded as a Taylor series from their value on the mean scattering surface. Formulation of perturbation theory almost always assumes that this mean scattering surface is a plane. Kirchhoff approximation requires that the scattering interface be relatively smooth in the sense that its curvature radii must not be much smaller than the acoustic wavelength. This approximation is used in conjunction with an integral formula to express the scattered field at some distance from a scatterer in terms of the approximated surface field. Scattering from within the near-specular angular range is handled by the Kirchhoff approximation involving large-scale waves, whereas scattering away from the specular range is handled by the perturbation approximation, which involves small-scale waves [10-12]. However, for bottoms that are variously rough in terms of being both large and small relative to the acoustic wavelength, which is common for natural rough bottoms, these two classical approximations have been combined to form the composite roughness approximation [13]. The composite roughness approximation's primary drawback is that cross sections derived from the perturbation and Kirchhoff approximation must be matched over some angular transition range that also depends on scattering angle. Therefore, a method without this drawback was required, and Voronovich [14] developed the small slope approximation. The small slope approximation solves the

problems of a unified description of wave scattering at rough surfaces in the framework of a single method and, in a sense, unifies the perturbation and Kirchhoff approximations. This paper reports that the measured data were compared to two models. The APL-UW model is based on the composite approximation [15]. The NRL model is calculated by small slope approximation [16]. Table 1 illustrates some key points regarding the use of both NRL and APL-UW model.

Table 1. A comparison between APL-UW and NRL model.

	APL - UW	NRL
Frequency	10 - 100 kHz	1 - 10 kHz
Approximation	Composite App.	Small-Slope App.
Interface	Fluid	Elastic
Classification of the sediment	Bulk grain size	Sediment name
Bottom Parameter	0.5 ϕ	Sand
Density ratio	2.231	2.0
Sound speed ratio	1.2503	1.2
Loss parameter	0.01638	0.005
Spectral exponent	3.25	3.3
Spectral strength	0.0069	0.006957

III. Laboratory tests of bistatic scattering

The tests were performed in a water tank at Ocean Acoustic Laboratory in Hanyang University. The dimensions of tank were 5 m \times 5 m \times 5 m. In consideration of effects of multipath interference, no four sides are parallel and the volume of the tank was about 125 m³. For measurements of bottom scattering, the tank was filled with 0.5 m - thick - sandy sediments to mimic the conditions similar to the real ocean (Fig. 1).

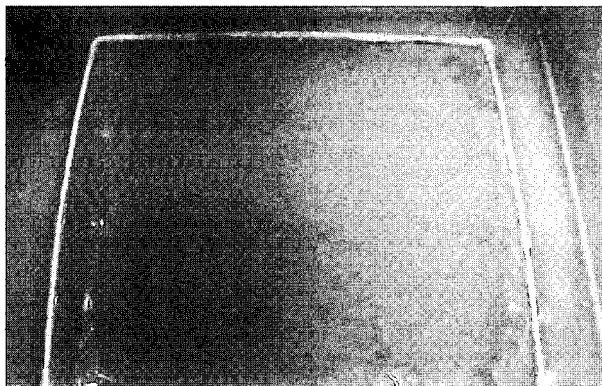


Figure 1. 4 m \times 4 m \times 0.5 m coarse sandy bottom at the Ocean Acoustic Laboratory.

3.1. Azimuthal distribution scattering pattern from artificially corrugated surface.

Azimuthal distribution scattering pattern measurements were made using one of OAL measurement system. Fig. 2 shows the experimental layout and bistatic geometry for measurement. θ_{gra} , the grazing angle, is an angle between incident wave and a surface. θ_{scat} , the scattering angle, is called between scattered wave and a surface. ϕ_{bi} is the bistatic angle between the incident wave and the scattered wave. If the bistatic angle is equal to 0°, then the bistatic case becomes the backscattering case. Directional transducer was located at depths of 210 cm and the grazing angle was fixed at 36°. The measurements were made using 0.4-ms-long CW pulses with 120 kHz frequency. The receiver was RESON 4104 omni-directional hydrophone that is located at the specular angle and subsequently rotated clockwise by 360°. In other words, grazing and scattering angles were fixed while bistatic angles changed. Each measurement set consisted of 80 pings with three repetitions. The received signals were averaged. The source level was 192.1 dB re 1 μ A at 1 m and receiving sensitivity was -3.8 dB re 1V/1 μ A. Receiving signals were digitized through 12-bit A/D converter and digitally filtered to remove noise. The sound velocity profile obtained by CTD (SB-19) gave an average sound velocity of 1460 m/s.

An artificially corrugated surface has varying impedance to measuring the scattering pattern. The artificially corrugated surface used in this study consisted of half circles with a radius 1.5 cm (Fig. 3). This means that the surface scattering will be

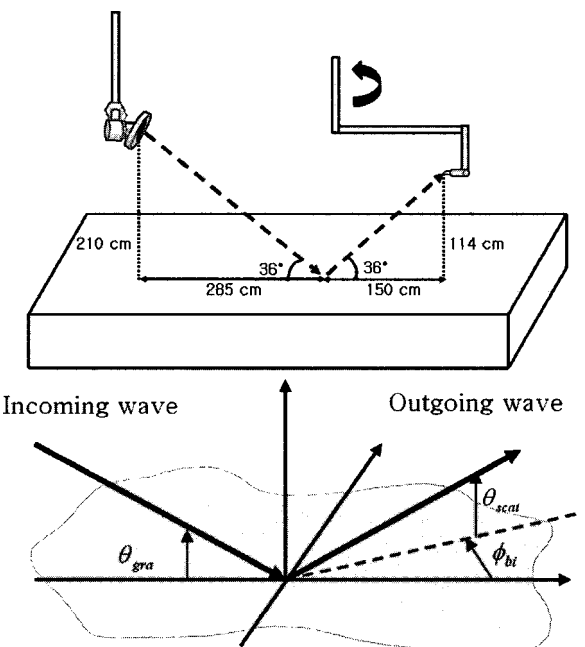


Figure 2. Experimental layout and Bistatic geometry.

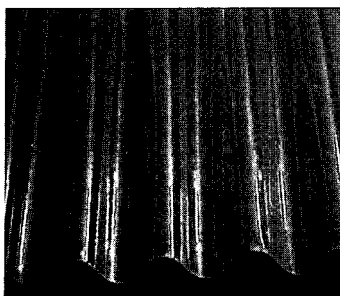


Figure 3. Artificially corrugated surface ($\rho c = 3.2 \times 10^6$).

mainly in the specular direction of the tangent plane. The Kirchhoff theory applies because the Rayleigh parameter is much larger than one for grazing angles of 36° . It is easy to change the direction of the artificial surface corrugations. The first measurement consisted of three parts (Fig. 4). The first two took measurements with the corrugated surface installed both transverse to the direction of incident wave and longitudinal to the direction of incident wave. The last measurement had a skew angle of about 45° (the angle between the corrugated surface and the incident wave). The artificially corrugated surface was located on the sediment. Its measured scattering pattern was compared to that of the flat sand sediment.

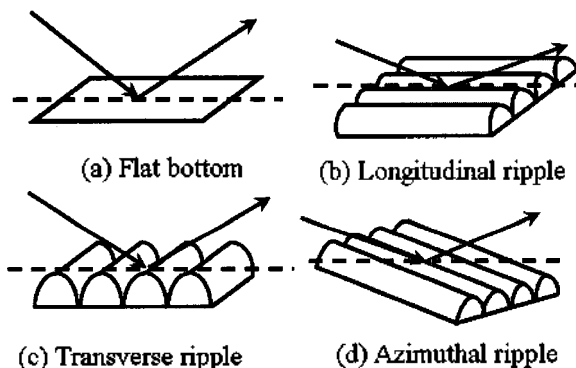


Figure 4. The artificially corrugated surface has three types: (a) flat, (b) longitudinal, (c) transverse, (d) azimuthal.

3.2. Azimuthal distribution scattering strength from a corrugated sediment

The second measurement was similar to those described in Sec.

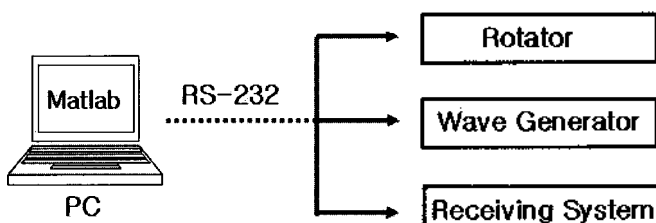


Figure 5. ARRS (Auto Rotating and Receiving System).

Table 2. Experimental parameters used to collect the scatterer signals.

Grazing and Scattering angle(°)	Transducer Height(m)	Receiver Height(m)
33	1.82	0.9
37	2.10	1.05
41	2.43	1.21

3.1. These measurements were made using Auto Rotating and Receiving System (ARRS), employing a single transmitter mounted on a steel pipe and a hydrophone fixed on a rotator. The transmitted signals were 0.4 ms long CW pulses with a frequency range from 50 to 100 kHz, with an increment of 1 kHz. The rotator was revolved 180° in 140 steps of 1.3° . The hydrophone was rotated one step clockwise, and the signals were transmitted and received 10 seconds later. The received signals were digitized at a 500-kHz rate through a 12-bit A/D converter and were bandpass filtered for noise removal. All system operations were under the control of a computer by RS-232.

The transmitter's 3 dB beam width was 14.6° . Both the grazing angles and scattering angles were 33° , 37° and 41° . All measurements were made at specular angles.

The source signals consisted of 10 pulses transmitted at 0.5s intervals. The sediment upper 5 cm were sampling for grain size measurement. Bulk measurement of the samples revealed an average grain size of 1.5Φ . The water sound speed was 1460 m/s, which gave a critical angle of approximately 37° . The first measurement was made on the flat sediment. A second measurement was performed from corrugated sediment to simulate sand ripple. The corrugated sediment was made with a triangular shaped rake as in Fig. 6.

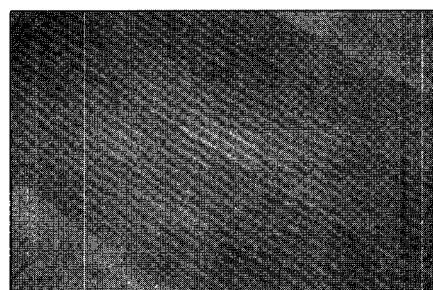


Figure 6. Photograph of corrugated sediment.

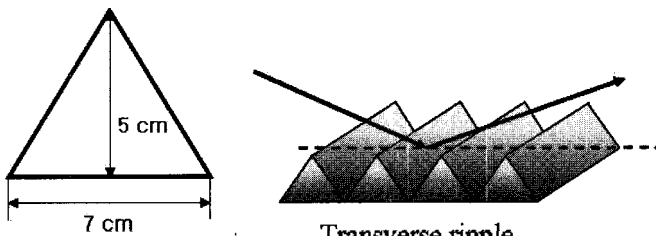


Figure 7. Single corrugated sediment cross section dimensions.

The troughs were made transverse to the direction of the incident wave as in Fig. 4. Fig. 7 is the cross sectional shape of single corrugated sediment with height 5 cm and base 7 cm, as used in this test. Thus the Rayleigh parameter is much larger than 1 for all three grazing angles of 33°, 37° and 41°.

3.3. Data analysis

There are two fundamental configurations of active sonar. Monostatic sonar transmits a pulse, which interacts with a target, resulting in an echo, which returns to the transmitter. For bistatic sonar, the receiver is in a different location than the transmitter. In the monostatic case, the transmission loss is $2TL$ where TL is the one-way transmission loss. In the bistatic case, the transmission loss is TL_1+TL_2 where the transmission loss is the sum over paths from the transmitter to the target and from the target to the receiver.

The bistatic scattering strength is given by

$$RL = SL - TL_1 - TL_2 + SS + 10 \log A \quad (1)$$

Where RL is the received level, SL is the source level at 1 m, TL is the transmission loss along R , and A is the ensonified area. In case of monostatic scattering, the ensonified is calculated as follows

$$A = r\Phi \frac{c\tau}{2\cos\theta} \quad (2)$$

Where r is the horizontal range from the source to scatterer, Φ is the effective horizontal beamwidth of the transducer, θ is the grazing angle, c is the water sound speed and τ is the pulse length[17].

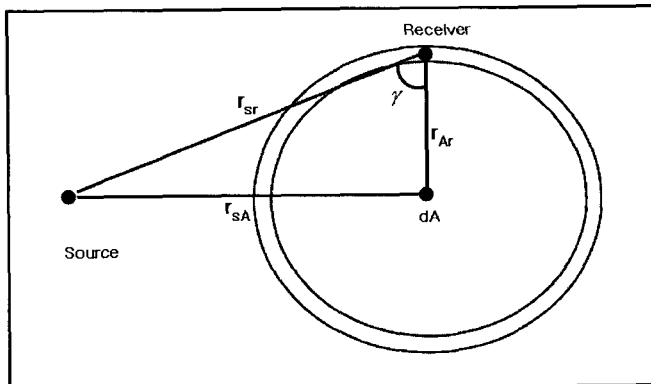


Figure 8. Notation and geometry of bistatic configuration for one scattering path.

IV. Results of laboratory tests

4.1. Azimuthal distribution scattering pattern for artificially corrugated surface

Fig. 9 shows a time series of averaged pulse voltages. It clearly shows the bottom-scattering arrivals, which can be verified from geometric calculations of the arrival times. Reverberation level is calculated as an average of the received signal over the duration of the pulse.

Azimuthal distribution scattering strengths were calculated as a function of bistatic angle and scattered angle. For the scattering pattern measurement, the scattering strength was normalized by the maximum scattering strength. The objective of this measurement was to obtain experimental values for the azimuthal distribution scattering pattern and compare them to the APL-UW model output. In Fig. 10, the outputs, scattering strengths, have different magnitudes because scattering patterns of each longitudinal, transverse, azimuthal direction were measured with artificially corrugated bottom and the scattering pattern of flat bottom was conducted with flat sand bottom. When plotted together, it's hard to see much detail in the smaller response. So all of data, scattering strengths, were normalized and normalizing displays each curve variations clearly. Data of the flat case graph between Fig. 10 (a) and Fig. 10 (b-d) is different. The flat case graphs of Figure 10 (b-d) show the results of normalized scattering strengths from flat and bottom to compare the scattering pattern between flat bottom and each corrugated bottom. Meanwhile, in Fig. 10 (a), the flat case measured data aren't normalized to compare with the model.

Comparisons between model and measured scattering pattern are plotted as a function of bistatic angle in Fig. 10 (a). The

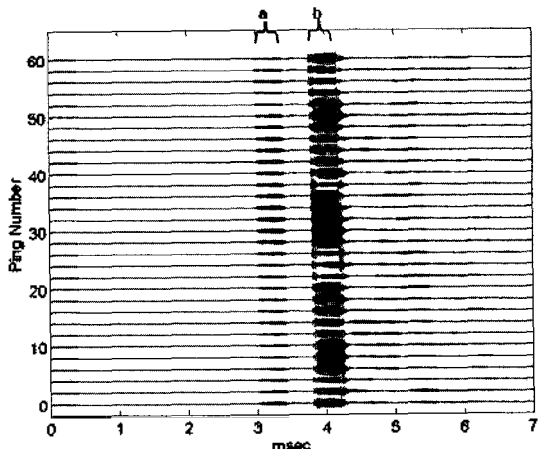


Figure 9. The measured signals at corrugated surface.
(a) direct path, (b) surface scattering path.

model calculation is the solid line while the stars represent the flat sediment values. On the flat sediment, the specular scattering angle showed the strongest forward scattering strength. In all directions there is little difference between the model and the data. The different impedance may be the cause of the difference in the corrugated surface. The stars represent the flat sediment while the points represent the longitudinal direction in Fig. 10 (b). The azimuthal scattering variations are a function of the bistatic angles. In the longitudinal direction the forward scattering is strongest, and the side scattering and near backscattering are stronger than in the flat direction. This scattering pattern is similar to the flat sediment. Fig. 10 (c) shows that the stars are the flat sediment and the points represent the transverse direction. The forward scattering remains strong. The backscattering here is much stronger than from the flat sediment. Fig. 10 (d) shows the measured azimuthal distribution scattering pattern as a function of the bistatic angles. This scattering pattern was a strong directional scattering, which is equal to the corrugated direction. Overall scattering strength patterns depend on the corrugated surface direction.

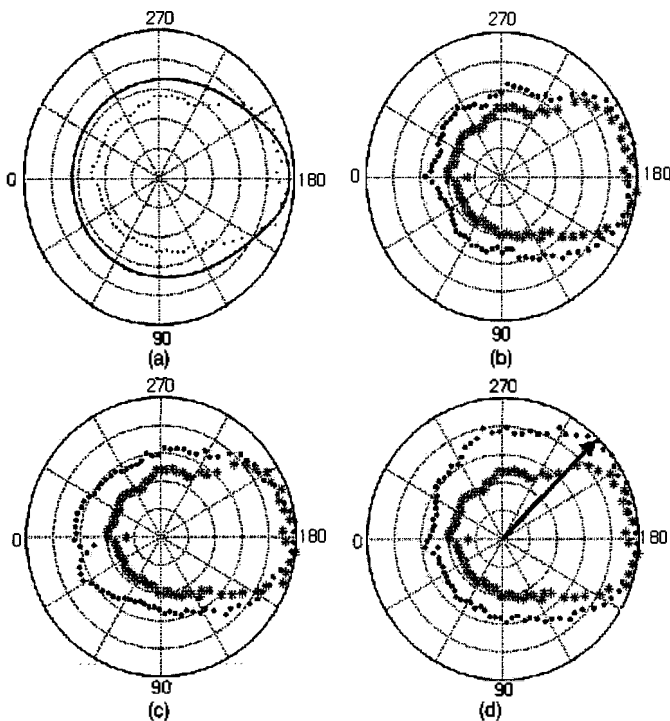


Figure 10. The scattering pattern of (a) flat, (b) longitudinal direction, (c) transverse direction, (d) azimuthal direction.

4.2. Azimuthal distribution scattering strength from a corrugated sediment

In order to compare the measured scattering strengths to the model, both the APL-UW and the NRL models were used.

Bottom parameters including sediment sound speed, density and bottom roughness were estimated from the empirical relationship in Table 1. The critical angle, 37° , is calculated from the ratio of the water sound speed to the sediment sound speed; therefore, the measurements were performed using three grazing angles: 33° (lower than critical angle), 37° (critical angle) and 41° (higher than critical angle). Fig. 11 shows the comparison between the flat sediment measured data and the models as a function of the bistatic angles. The points represent the data. The solid line represents the results of APL-UW model. The dashed line shows the results of the NRL-model. The APL-model is to the same as the NRL model at the specular region. However, away from the specular region, the NRL model outputs decrease more rapidly than those of the APL-UW model. For a grazing angle of 33° , both model outputs and the measured data show favorable comparisons for near forward scattering. However, the scattering strength variations are between 3 and 10 dB. For grazing angles of 37° and 41° , the measured scattering strengths were closer to the outputs from the NRL model than to the APL-UW model. However, overall measured scattering strengths were 4 ~ 8 dB lower than the NRL model outputs. The effect was equal to both 70 and 90 kHz.

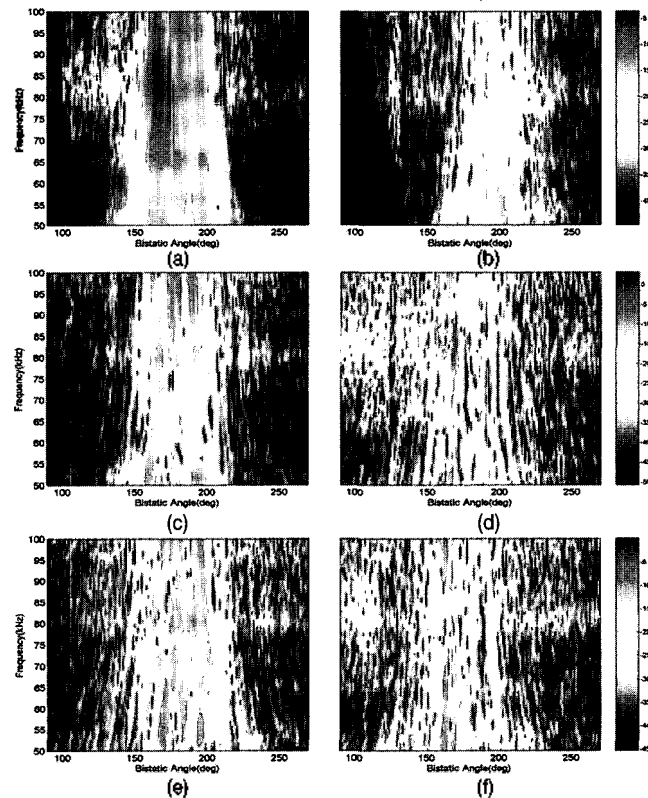


Figure 11. The measured scattering strengths : the left side is flat bottom, the right side is artificially rippled bottom, (a) and (b) grazing angles 33° , (c) and (d) grazing angle 37° , (e) and (f) grazing angled 41° .

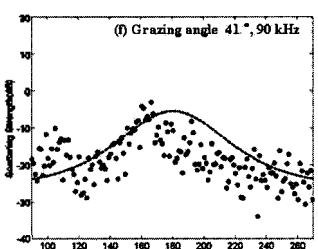
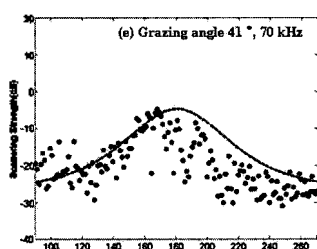
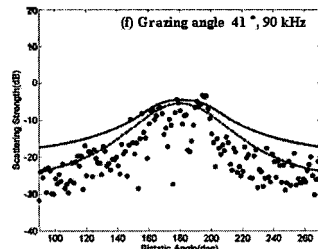
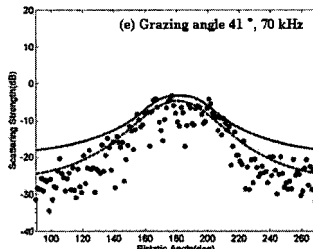
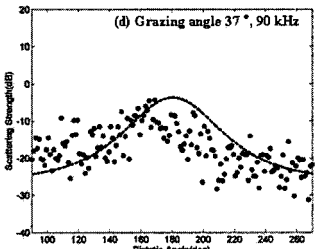
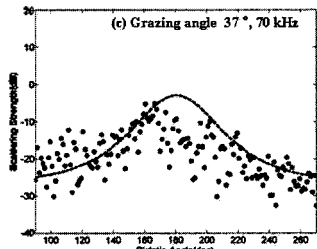
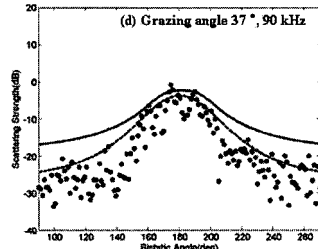
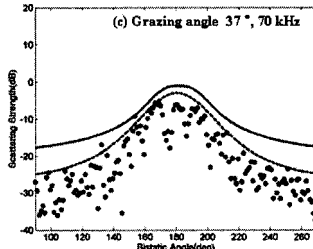
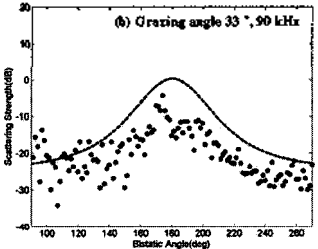
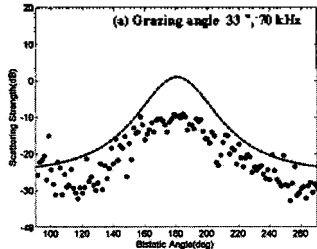
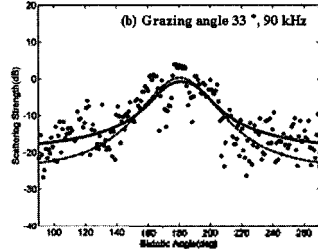
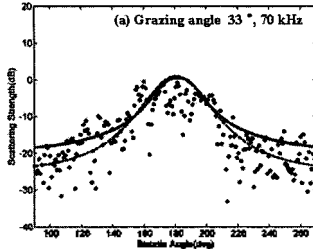


Figure 11. Comparison of predictions by APL-UW model (solid line), NRL model (dashed line) and measured data (point) at flat bottom.

Fig. 12 compares the measured data from a corrugated sediment surface to the result calculated by the NRL model as a function of bistatic angles. The points represent the data. The dashed line is the result calculated from the NRL-model. For the 33° angle, the measured scattering strengths were over 10 dB lower than the NRL model showed at the specular region. Away from the specular region, the measured scattering strengths were 3 ~ 5 dB lower than the NRL model. For the 37° and the 41° angles, the measured scattering strengths were about 5 dB lower than the NRL model at the specular region. Fig. 13 shows that the scattering strengths were measured with a frequency range from 50 to 100 kHz.

The frequency dependency of the scattering strengths was surely related to the rms height of the bottom roughness. But it wasn't discussed in this study as this time our purpose of the study is experimentally to measure the bistatic scattering pattern from both flat and corrugated bottom (artificial and sand) with grazing angles, as well as the measured scattering data are compared with two existing scattering models.

The result indicates that the forward scattering strengths measured at a grazing angle of 33° were more strongly affected

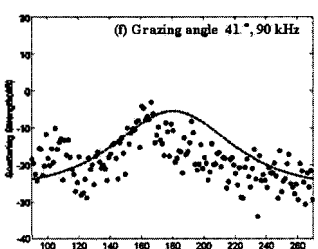
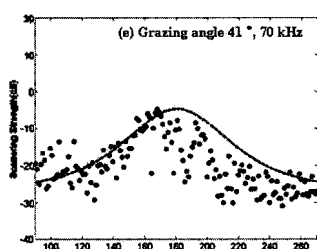
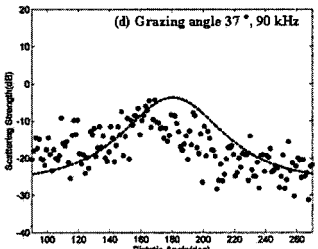
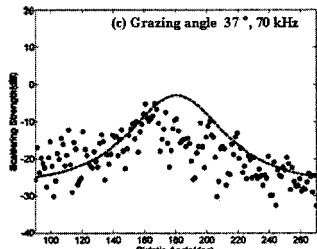
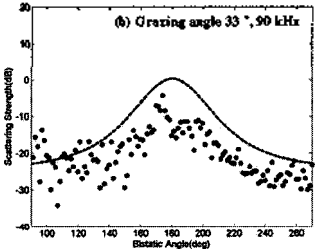
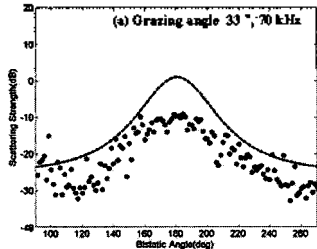
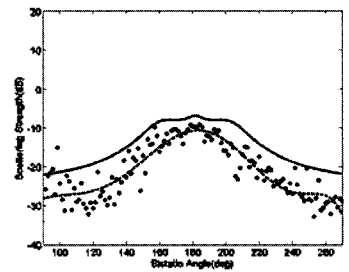
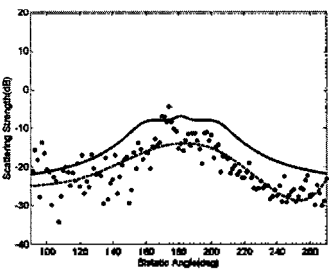


Figure 12. Comparison of predictions by NRL model (dashed line) and measured data (point) at artificially ripple bottom.

than were the other grazing angles. The power spectral representation of interface roughness often presents a useful description of roughness for modeling high-frequency acoustic scattering. The bottom roughness is evaluated for height fluctuations as a function of spatial frequency with the roughness power spectrum. Two parameters, γ_2 (the spectral exponent), w_2 (the spectral strength parameters), are used as parameters of roughness power spectrum in this model. And the proposed values of two parameters in the model are limited for the bottom of the isotropic two-dimensional relief spectrum. The models and the measured data are different because the models used an



(a)



(b)

Figure 14. Comparison of the modified NRL model (solid line), measured data (point) and dotted line was plotted with the data at the corrugated sediment: (a) 70 kHz, (b) 90 kHz.

isotropic correlation function for sediment roughness in the scattering calculations. The isotropic correlation function consists of w_2 and γ_2 . These constants are derived from sediment names or bulk size. The model, which used the constants, didn't consider the corrugated surface effect. In order to consider the corrugated surface, the constants were varied in the NRL model. Fig. 14 shows those results. The points represent the data and the dotted line was plotted with those data. The solid line shows the modified model outputs. The results show that the modified NRL model was more similar to the measured data from corrugated sediment surface.

V. Summary and Conclusions

This paper explains azimuthal distribution scattering from artificially corrugated surfaces. The goal of this paper was to understand the scattered energy distributions from the direction of corrugated surfaces. First the azimuthal scattering pattern was measured from an artificially corrugated surface. Second, scattering strengths were measured from flat sediment and corrugated sediment. The measurements were made at three fixed grazing angles: 33°, 37° and 41°. The corrugated sediment was made transverse to the direction of the incident wave.

The first measurement indicates that the scattering patterns depend on the relations between the corrugated surface and the direction of the incident wave. For installed longitudinal to the direction of incident wave, the scattering pattern is similar to the flat sediment scattering pattern. For installed transverse to the direction of the incident wave, the scattering pattern showed strong backward scattering. For installed azimuthal to the direction of incident wave, the scattering pattern had about 45° which equals the angle between the corrugated surface and the direction of the incident wave.

In the second measurement, the data measured from the flat sediment were compared to the APL-UW and the NRL models. The NRL model output shows a more favorable comparison to the measurements than does the APL-UW model. With a corrugated sediment the scattering strengths at a grazing angle of 33° were about 10 dB lower than the model output near the specular region. Away from the specular region the measured scattering strengths are 3 ~ 5 dB lower than the NRL model. At grazing angles of 37° and 41°, the measured scattering strengths were about 5 dB lower than the model output. On the corrugated

sediment, the model and the measured data differ at a grazing angle of 33° because the models used an isotropic wave spectrum of sediment roughness in the scattering calculations. The isotropic wave spectrum consists of w_2 and γ_2 . These constants are derived from sediment names or bulk size. The model which used these constants didn't consider the corrugated surface effect. In order to consider the corrugated surface, the constants were varied in the NRL model. To calculate the model with accuracy, the isotropic wave spectrum was modified at corrugated surfaces such as ripples.

In conclusion, the azimuthal bistatic scattering characteristics from the corrugated sediment are important. It is especially sensitive at a grazing angle lower than the critical angle. Also, scattering strength and scattering pattern were affected by the relations between the corrugated surface and the direction of the incident wave. In case of the corrugated sediment, the model results differ from the measured data. To accurately calculate the model, the isotropic wave spectrum is modified at corrugated surfaces such as ripples.

In the future, the isotropic wave spectrum will be derived from other methods. Recently, the availability of cameras and advances in PC-based processing of digital images has greatly improved our ability to estimate the sea-floor roughness. The high-resolution data obtained with this system must be used to evaluate the impact of the directional wave spectrum on scattering.

References

1. Xavier Lurton., *An Introduction to Underwater Acoustics*, (Chichester, UK, 2002)
2. Stanic, S., E. Kennedy, and R. I. Ray, "High-frequency bistatic reverberation from a smooth ocean bottom," *J. Acoust. Soc. Am.*, **93**, 2633-2638, 1993.
3. Boehme, H. N. P. Chotiros, L. D. Rolleigh, S. P. Pitt, A. L. Garcia, T. G. Goldsberry, and R. A. Lamb, "Acoustic backscattering at low grazing angles from the ocean bottom, Part I. Bottom backscattering strength," *J. Acoust. Soc. Am.*, **77**, 962-974, 1985.
4. Nolle, A. W. and W. A. Hoyer, J. F. Mifsud, W. R. Runyan, and M. B. Ward, "Acoustical properties of water-filled sands," *J. Acoust. Soc. Am.*, **35**, 1394-1408, 1963.
5. Urick, R. J., "Side scattering of sound in shallow water" *J. Acoust. Soc. Am.*, **32**, 351-356, 1959.
6. Choi, J. W., J. Na, K. Park, K. Yoon, J. S. Park, and Y. N. Na, "Measurements of high-frequency sea surface backscattering signals," *J. Acoust. Soc. Korea*, **21** (4) 421-429, 2002 (in Korean).
7. Medwin, H. and C. S. Clay *Fundamentals of Acoustical Oceanography*, (Academic Press, Boston, 1998)
8. Bass, F. G. and I. M. Fuks, *Wave Scattering From Statistically Rough*

- Surfaces, Tergamon*, (New York, 1979)
9. Eckart, C., "The scattering of sound from the sea surface," *J. Acoust. Soc. Am.*, **25**, 566-570, 1953.
 10. Dahl, P. H., "On bistatic sea surface scattering: Field measurements and modeling," *J. Acoust. Soc. Am.*, **105**, 2155-2169, 1999.
 11. Thorsos, E. I., "The validity of the Kirchhoff approximation for rough surface scattering using a Gaussian roughness spectrum," *J. Acoust. Soc. Am.*, **83**, 78-92, 1988.
 12. Williams, N. J., "An experiment to measure low frequency acoustic backscatter from the ocean wave surface-The acoustic surface reverberation experiment, ASREX," Ph.D. thesis, University of Miami, 1996.
 13. McDaniel, S. T. and A. D. Gorman, "An examination of the composite-roughness scattering model," *J. Acoust. Soc. Am.*, **73**, 1476-1486, 1983.
 14. Voronovich, A. G., *Wave Scattering from Rough Surfaces*, Springer-Verlag, (New York, 1993)
 15. APL-UW "High-Frequency Ocean Environmental Acoustic Models Handbook", Ch. IV, Bottom, APL-UW TR 9407, October 1994.
 16. NRL, "Broadband Models for Predicting Bistatic Bottom, Surface, and Volume Scattering Strengths," Technical Report NRL/FL/7100-02-10, 042, 2002.
 17. Cox, H. "Fundamentals of bistatic active sonar," in Underwater Acoustic Data Processing, edited by Y. T. Chan, Kluwer Academic Publishers, Dordrecht, 1988.

[Profile]

•Hongsang Cho



Hongsang Cho received the B.S. and M.S. degrees in earth and marine sciences in 2004 and 2006, respectively, from Hanyang University, Korea. His research interests include bottom scattering and modeling.

•Hyungsul La

The Journal of the Acoustical Society of Korea, Vol.24, No.2, 2005.

•Kwan-seob Youn

The Journal of the Acoustical Society of Korea, Vol.23, No.4, 2004.

•Jungyul Na

The Journal of the Acoustical Society of Korea, Vol.23, No.4, 2004.

•Bong-chae Kim

Bong-chae Kim received the B.S. degree in fisheries science from National Fisheries University of Pusan in 1977, and the Master and the Doctor of Engineering degrees in underwater acoustics from Tokai University, Japan, in 1985 and 1988, respectively. In 1990 he joined the Korea Ocean Research and Development Institute as a senior research scientist. His current research interests include sound propagation in the sea, oceanic ambient noise, and ocean acoustic tomography.